Advances in Sustainable Energies & Environment, 1 (2026) 3, 14 – 28

Advances in Sustainable Energies & Environment

Journal homepage: https://A-SEE.MazUST.ac.ir/

Research Article

Structural and environmental effects of the application of Autoclaved Aerated Concrete blocks in the Intel-Deck roof system

Sanaan Nasri [a], Somayeh Mollaei [a*], Davoud Jahani[b], Mohammad Javad Samereh[a]

[a] *Department of Civil Engineering, University of Bonab, Bonab, Iran*
[b] *Department of Mechanical Engineering, University of Bonab, Bonab, Iran*

Article Info

Article history:
Received: 2025-11-11
Revised: 2026-05-05
Accepted: 2026-05-16
Published: 2026-07-01

Keywords:
Intel-Deck Roof System;
AAC Blocks;
Life Cycle Assessment;
Environmental Effects.

Abstract

This study investigates the feasibility of replacing conventional upper and lower clay blocks in the Intel-Deck roof system with autoclaved aerated concrete (AAC) units, evaluating both structural performance under lateral loading and environmental sustainability indicators. Construction waste management and building energy performance scenarios for AAC and traditional clay bricks were modeled using DesignBuilder through energy simulation and waste-related output assessment. The resulting life cycle inventory data were analyzed in openLCA using a life cycle assessment (LCA) framework based on the TRACI impact assessment methodology to quantify environmental burdens. From a structural perspective, reinforced concrete frames incorporating AAC-based Intel-Deck slabs were modeled in ETABS using linear static analysis to evaluate story drifts, internal forces, and reinforcement demand. Furthermore, three-dimensional finite element modeling was carried out in ABAQUS under quasi-static lateral loading conditions using nonlinear analysis to determine the equivalent slab thickness of the AAC-integrated roof system. The results indicate that clay brick construction exhibits higher global warming potential, ozone depletion, and fossil fuel consumption compared to AAC, while nonlinear finite element analysis yields an equivalent slab thickness of approximately 15 cm for structural equivalency.

Graphical Abstract

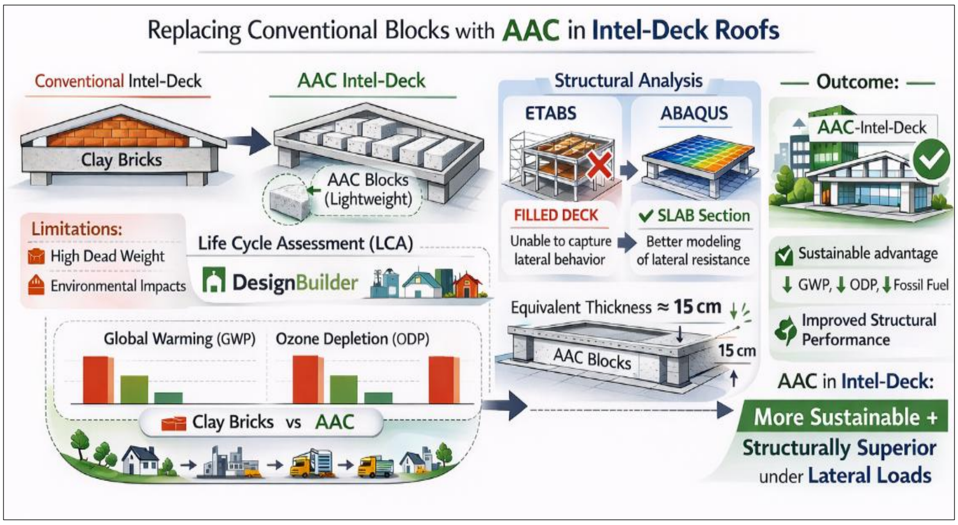

*** Corresponding author:**
E-mail address: *s.mollaei@ubonab.ac.ir*

Cite this article as:
Nasri, S., Mollaei, S., Jahani, D., & Samereh, M.J. (2026). Structural and environmental effects of the application of Autoclaved Aerated Concrete blocks in the Intel-Deck roof system. *Advances in Sustainable Energies & Environment 1 (3) 14 - 28.* https://doi.org/10.22034/a-see.2026.2077488.1018

1. Introduction

In recent years, increased competition and the drive for progress have led many countries to focus their activities and capabilities on infrastructure industries, especially the construction industry, and one of the most notable activities in this industry has been innovation in the field of slab and roof systems. Among these innovations, biaxial voided slab systems have been introduced as an advanced structural solution aimed at reducing self-weight while maintaining structural efficiency through the incorporation of strategically spaced voids within the concrete section. Recent experimental and numerical investigations have demonstrated that the size and spacing of void formers significantly influence the flexural stiffness and ultimate load-carrying capacity of such systems, highlighting the importance of geometric parameters in their structural performance [1,2]. According to Figure 1, the Intel-Deck roof uses an I-shaped cross-section, which improves mechanical properties and saves on rebar percentage, as well as reducing long-term deflection. In this roof system, two types of blocks are used in the lower and upper parts of the slab, which are usually made of lightweight concrete and polystyrene.

Due to the advantages of using lightweight concretes, these materials have been recognized as one of the most widely used construction materials in recent years and the demand for their use is increasing [3]. Foam concrete is considered one of the most important types of lightweight concrete. Foam concrete, which is created by creating foam or releasing gas bubbles in the cement paste during its manufacture, is divided into two general categories; foam concrete and autoclave aerated concrete (AAC) [4,5]. Autoclaved aerated concrete (AAC) has attracted considerable attention as a lightweight construction material due to its porous structure and favorable thermal and acoustic properties. Experimental studies indicate that the mechanical performance of AAC masonry depends significantly on block–mortar interaction, while advanced ultra-lightweight formulations have achieved improved thermal efficiency through microstructural regulation and optimized tobermorite formation. The geometry and distribution of air pores strongly influence stiffness, strength, and durability, and long-term exposure to moisture further highlights the importance of durability considerations in porous mineral materials. Recent research has also focused on enhancing sustainability through the incorporation of industrial by-products and alternative pozzolanic materials, which affect hydration mechanisms, phase transformation, and autoclaving efficiency. At the structural level, investigations on AAC wall joints demonstrate that connection detailing plays a critical role in load-bearing capacity and cracking behavior, emphasizing the need for an integrated understanding of material characteristics and structural performance [6-13]. A study by Fouad et al. [14] on the environmental impact assessment of AAC materials in the United States showed that the efficiency of these materials is higher than that of wood and conventional concrete. Shi et al. [15] and Reyes-Quijije et al. [16] also conducted a similar study in China and Ecuador, respectively, in which they also reported high energy efficiency in the production, transportation and consumption of AAC materials compared to similar construction materials. In another work by Raj et al. [17], studies were conducted on the energy consumption and environmental impacts of all stages of AAC block production.

Recent international studies have increasingly evaluated autoclaved aerated concrete (AAC) from environmental, economic, and thermal performance perspectives. Life cycle assessment (LCA) investigations of AAC production processes have identified key contributors to environmental impacts, particularly cement production, lime processing, slurry preparation, and steam curing, which significantly influence ecotoxicity and resource depletion indicators [10]. Comparative analyses between AAC and fired-brick wall systems further demonstrate that while AAC walls generally exhibit higher thermal resistance (R-values), fired-brick walls may present lower total environmental burdens and life cycle costs under certain configurations [18]. Multi-criteria decision-making approaches, including Analytic Hierarchy Process (AHP), highlight that optimal wall selection depends on balancing environmental impacts, embodied energy, thermal performance, and economic factors [18].

At the building-envelope scale, wall systems play a dominant role in operational energy demand, accounting for a substantial portion of total building energy consumption [19]. Experimental studies conducted under real climatic conditions indicate that AAC and AAC sandwich wall systems significantly reduce indoor temperature fluctuations, heat load levels, and CO_2 emissions compared to conventional brick walls [20].

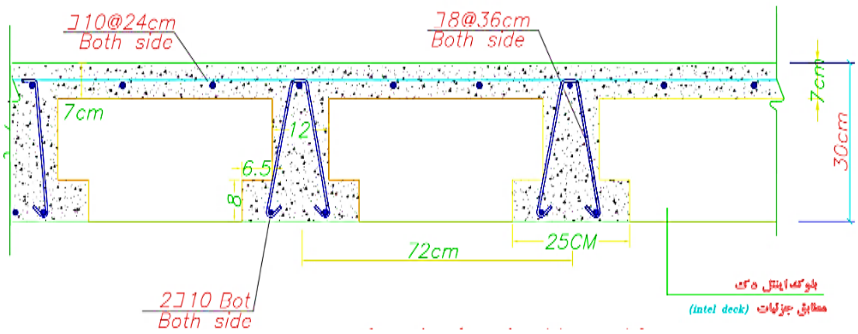

Fig. 1. Intel-Deck roof system details Studied here

In particular, AAC sandwich configurations enhance thermal inertia and energy efficiency, achieving considerable long-term energy savings over a typical building life cycle [20,21]. Dynamic thermal response analyses further confirm that AAC-based insulated wall systems effectively attenuate temperature amplitudes and reduce heat consumption indices, reinforcing their potential in low-carbon and energy-efficient building design [21].

What motivated this research was one of the common implementation problems in Intel-Deck roofing systems. According to Figure 2, in the usual case, the lower blocks of the Intel-Deck roof are made of lightweight concrete, and the upper blocks are polystyrene. Fracture of polystyrene blocks during the construction, concrete pressure, and the weight of the rebars is a common construction problem in Intel-Deck roofs. On the other hand, the release of toxic gases under high temperatures (in a fire) is another disadvantage of polystyrene blocks. In terms of construction problems, fracture, crushing, and throwing of the lower blocks is also a frequent problem [2].

The main objective of this study is to investigate the feasibility of replacing the conventional upper and lower blocks in the Intel-Deck roof system with autoclaved aerated concrete (AAC) units. The structural performance of the modified system was evaluated and compared with the conventional configuration, with particular emphasis on lateral load behavior. In parallel, the environmental justification of AAC application was assessed based on sustainable development indicators in comparison with traditional clay brick materials. A SWOT (Strengths, Weaknesses, Opportunities & Threats) framework was first employed to perform a qualitative technical and economic assessment of AAC and brick systems. Subsequently, building energy simulation and construction waste management scenarios were modeled using DesignBuilder software to quantify energy consumption and waste-related outputs. The resulting life cycle inventory data were further analyzed through environmental impact assessment using the openLCA platform based on the TRACI methodology.

From a structural perspective, linear static analysis and drift evaluation of reinforced concrete frames incorporating Intel-Deck slabs were carried out in ETABS software, considering different diaphragm modeling approaches. Furthermore, nonlinear three-dimensional finite element analysis (FEM) under quasi-static lateral loading was performed in ABAQUS to determine the equivalent slab thickness corresponding to the AAC-based roof system. The integration of environmental assessment and advanced structural modeling provides a comprehensive evaluation framework for assessing the structural and sustainability performance of AAC-integrated Intel-Deck systems.

2. Materials and methods

2-1. SWOT method

In this study, SWOT approach was used to evaluate the technical and economic features of AAC blocks. The general schematic of this method is shown in Figure 3. In general, SWOT method analyzes the internal and external environments and makes strategic decisions based on them. Here, first, the parameters examined in the SWOT analysis are introduced, and then a comparison is made of the materials used in the building.

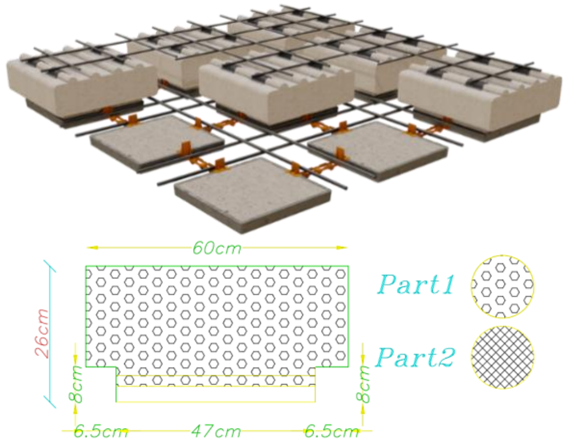

Fig.2. Details of the lower and upper blocks in a conventional Intel-Deck roof system

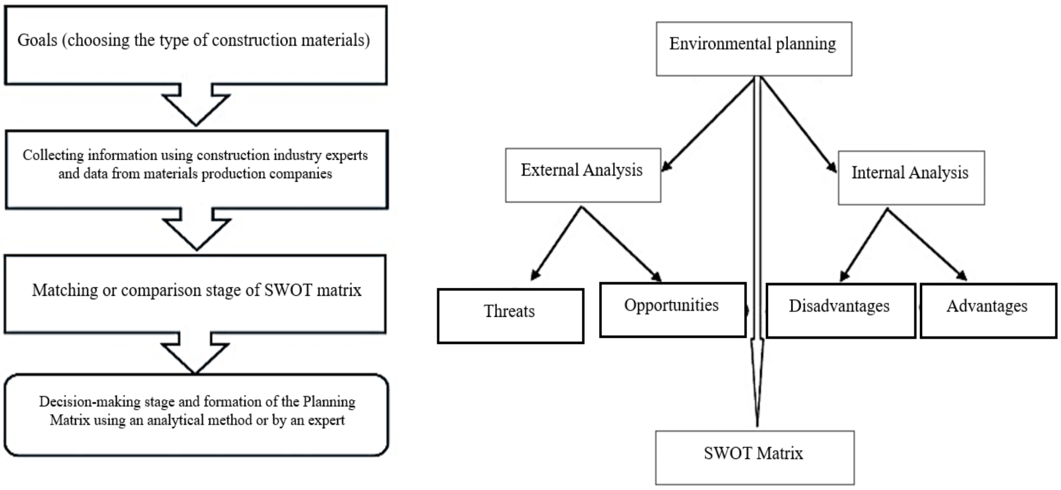

Fig.3. SWOT analysis framework.

The data used here is related to the information available in the studies and product specifications of Happho Company [22], which is a leading company in the world in the field of construction. In this study, in order to investigate and analyze the environmental impacts of ACC materials, various parameters were considered, including constituent materials, size variations, compressive strength, profitability, fire resistance, final product quality, sound insulation, energy storage, environmental compatibility, construction cost, connection process, availability, thermal insulation, contractor issues, tax issues, scope of application, and water absorption. It is obvious that some of these factors overlap with each other and other factors can also be used in comparative analyses; however, considering the previous research and also the consultation of experts in Iran's construction industry, these parameters were sufficient here.

In this study, to assess the environmental impacts of using AAC materials, a scenario was developed based on the data available in the region and standard data using DesignBuilder software [23]. The “region” refers to the local climate, weather conditions, and energy and construction characteristics associated with the geographical location under study. These include monthly average temperature, relative humidity, solar radiation, prevailing wind direction, local energy prices, dominant building types, and conventional construction systems. Such regional parameters are integrated within the BIM-based LCA framework to ensure consistency between climatic data, material inventories, and environmental databases at different levels of development (LOD). Climate data were obtained from regional meteorological sources and DesignBuilder weather files (EPW format), while construction-related information was derived from local case studies and municipal building archives [24]. Therefore, here the geographical location of Kermanshah province was considered and its climatic and construction data were considered as the main input of the model to perform a more accurate simulation. In the modeling in DesignBuilder software, two different scenarios of implementing Intel-Deck roofs were performed for energy consumption analysis and environmental assessment. Basically, input data have a key role in the accuracy, validity and applicability of DesignBuilder modeling results. In this study, data were extracted from two main sources; climatic-regional variables of the project location and physical and thermodynamic data of the materials used in two scenarios of traditional block and AAC. Here, the EPW climatic file of Kermanshah province was used. Finally, two scenarios for energy modeling and environmental analysis were defined in DesignBuilder software, including a building with perimeter walls and internal partitions made of clay bricks or made of AAC materials; Some of the key inputs are given in Table 1.

According to Table 1, the thickness of the roof block was considered equal in both scenarios to investigate the effect of the type of materials on thermal performance. AAC block has a lower density than traditional blocks, which leads to a reduction in the weight of the structure and improved thermal performance. AAC block has a lower thermal conductivity coefficient, which indicates its better thermal insulation. Also, the higher thermal capacity of AAC block helps maintain the internal temperature of the building. The lower value of the overall heat transfer coefficient U in the second scenario indicates a reduction in heat transfer through the roof. The reduction in energy consumption in the second scenario is due to the better thermal performance of AAC block. The reduction in greenhouse gas emissions in the second scenario is due to the reduction in energy consumption and the use of materials with a cleaner production process. Also, the maintenance costs of the building are higher if brick materials are used in the internal and external walls of the building than AAC materials because they require supplementary insulation.

Comparison of outputs such as energy consumption, emitted pollutants and thermal performance, the basis of environmental analysis, was performed in OPENLCA software. The amount of pollutants resulting from the recycling or waste disposal stages of each scenario and the energy consumed in them were calculated. Then, the obtained data were entered into the openLCA software [25] and the environmental impact assessment was performed using the TRACI (Tool for the Reduction and Assessment of Chemical and other environmental Impacts) [26] method. Finally, the results of the scenarios were compared and analyzed, and the results are presented in the next section of the article. In order to conduct the life cycle assessment of environmental sustainability in reinforced concrete buildings, two separate scenarios were defined based on quantitative and qualitative information of the building, construction specifications, construction equipment, biological processing, and thermal processing. After defining the scenarios, the amount of production and emission of pollutants (in water or air) was estimated by this model based on the amount of energy and fuel consumed, as well as the energy produced for each scenario. Finally, the outputs of this model were used in the initial life cycle inventory stage.

2-2. Life Cycle Inventory (LCI)

In this section, the information and outputs generated by DesignBuilder were transferred to the openLCA platform for environmental impact assessment.

Table 1. Input values of key parameters in the DesignBuilder model

Parameter	1st Senario: Brick material	2nd Senario: AAC blocks
Block thickness (cm)	25	25
Density (kg/m³)	1500-1900	300-800
Thermal conductivity coefficient (W/m·K)	1.4	0.12
Specific heat capacity (J/kg·K)	840	1000
Overall heat transfer coefficient (W/m²·K)	1.8	0.45
Annual energy consumption (kWh/m²)	180	130
Annual CO_2 emissions (kg/m²)	90	65

The integration was conducted within a BIM-based LCA framework, ensuring that the level of development (LOD) of building components was consistent with the level of detail available in the selected environmental databases. The open-LCA databases, developed according to internationally recognized life cycle assessment standards, provide comprehensive background data that enable reliable estimation of embodied environmental impacts when detailed material information becomes available. [24]. For energy sources and raw materials, generic data are available in various LCA databases. In this study, data related to diesel fuel production and emissions were used from the ELCD database, located in the openLCA life cycle assessment software, which is based on the Euro IV fuel standard and is also accepted here in Iran. The openLCA's database has all the flows (materials and energy) and processes necessary for modeling with different databases [25]. In order to calculate and evaluate the environmental impacts of the scenarios considered by the openLCA software, an environmental impact assessment using the TRACI method was performed on the data obtained from the life cycle inventory stage. Here, the data entered into the openLCA software were evaluated for environmental impacts based on the TRACI method at 10 different impact levels including acidity, ecosystem toxicity, eutrophication (excessive nutrient enrichment), global warming, human health in terms of carcinogenicity, human health in terms of non-carcinogenicity, ozone depletion, photochemical smog, fossil fuel depletion, and respiratory effects. In general, the results of life cycle inventory are assigned to different impact classes according to their type and impacts, and their final value is calculated by multiplying the amount of materials consumed or pollutants produced by a characteristic factor. The characteristic factor (coefficient) determines the impact potential of each pollutant relative to its average unit in each impact class.

2-3. Global Structural Analysis Using ETABS

In order to evaluate the structural effects of using AAC components in a structural roof system, in this study, a reference building frame was modeled by ETABS software using SLAB section for the roof and considering the contribution of the roof to the lateral stiffness of the structure.

The FILLED DECK section in the ETABS's library is a type of composite roof that is made of a metal trapezoidal deck with a set of shear studs which also is used as a mold during construction. Typically, users and engineers attempt to model the roof by introducing the structural dimensions of the Intel-Deck roof as input parameters of the FILLED DECK section and omitting the roof thickness. However, the effectiveness of this method in terms of the structural role of the Intel-Deck roof with AAC components needs to be examined. On the other hand, ETABS software has another section called SLAB that can model both bending and membrane behavior of the slab.

A plate-bending element has one translational degree of freedom perpendicular to the section plane and two rotational degrees of freedom about the horizontal axes at each node. In this study, three- and five-story reinforced concrete moment-resisting frame models incorporating the Intel-Deck roof system with AAC components were developed. Two diaphragm modeling approaches were considered: in the first configuration, the roof system was modeled using the FILLED DECK section definition, whereas in the second configuration, it was modeled using the SLAB section definition. The structural model consists of four columns in each principal direction (longitudinal and transverse), resulting in a total of sixteen columns with a center-to-center spacing of 4 m, with a typical story height of 3.2 m and a ground (pilot) story height of 3 m. A semi-rigid diaphragm was assigned to the floor system, and the base shear coefficient (C = 0.1178) was calculated in accordance with the Iranian Code of Practice for Seismic Resistant Design of Buildings (Standard No. 2800), 4th Edition [27].

The structural loading and definition of static load cases were determined in accordance with the National Building Regulations of Iran – Part 6 [28]. The dead load was considered as 470 kg/m² for the floors and 280 kg/m² for the roof, while the live load of the floors was taken as 200 kg/m². To account for internal partitions, a gravity load of 750 kg/m² was applied to the typical floors and 375 kg/m² to the top floor. According to the Iranian Seismic Code (Standard No. 2800), reduction factors of 0.35 for beam moment of inertia and 0.7 for column moment of inertia were adopted to account for concrete cracking effects. Table 2 presents the cross-sectional characteristics of the three- and five-story frame models.

2-4. Nonlinear 3D FEM Analysis in ABAQUS

To calibrate the equivalent thickness of the AAC-based Intel-Deck roof, a detailed three-dimensional finite element model was developed in ABAQUS. The modeling approach involved representing concrete elements as solid (3D) components and reinforcing bars as wire (linear) elements. Both the AAC-based and the conventional Intel-Deck systems were modeled. The interaction between various components was applied to the structure using the ‘Embedded Region’ tool. Gravitational loads were applied at the same magnitudes as in the ETABS linear analysis, and lateral loads were applied as acceleration time-histories corresponding to the Tabas earthquake, acting at the column bases. The boundary conditions were also determined in accordance with this type of lateral loading. The equivalent thickness was determined through a manual iterative calibration procedure, in which the slab thickness in the ETABS model was adjusted within practical and constructible limits, and nonlinear lateral analysis was repeated after each modification. The process continued until the difference in global lateral displacement between the two roof systems was less than or equal to 10%, and convergence was achieved after approxi-mately twenty iterations, indicating acceptable equivalence in global stiff-ness between the AAC-based and conventional configurat-ions. The geometric specifications of the afore-mentioned AAC blocks are presented according to Figure 2 provided earlier, while the specifications of the concrete joists and the final assembled roof geometry are provided in Figure 4. The geometric specifications of the proposed roof are presented in the images provided below.

Table 2. Details of the cross-sectional members of the 3rd and 5th floor frames in this study

Geometry	Beams reinforcement	Beams dimension (cm)	Geometry	Columns reinforcement	Columns dimension (cm)	Floor no.	
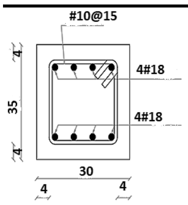	4ϕ18t; 4ϕ18b; Φ10@15cm; Φ10@7.5cm	30×35 30×35 30×35	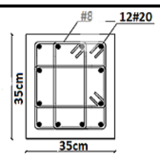	12ϕ20; ϕ8@10cm; ϕ8@20cm	35×40 35×40 35×40	1 2 3	3-story frame
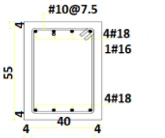	4ϕ18t+1ϕ16t; 4ϕ18b; 4ϕ18b+2ϕ16b; Φ10@15cm; Φ10@7.5cm	40×50	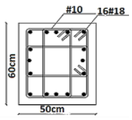	16ϕ18; Φ10@10cm; Φ10@20cm	60×50	1	5-story frame
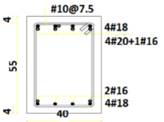		40×50	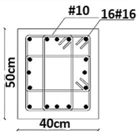	16ϕ16; Φ10@10cm; Φ10@20cm	50×40	2	
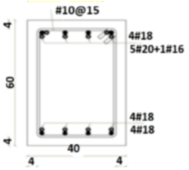	4ϕ18t+5ϕ20t; 4ϕ18b+4ϕ18b; Φ10@15cm; Φ10@7.5cm	40×60	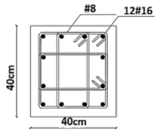	12ϕ16; Φ8@10cm; Φ8@20cm	40×40	3 4	
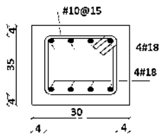	4ϕ18t; 4ϕ18b; Φ10@15cm; Φ10@7.5cm	40×60 30×35	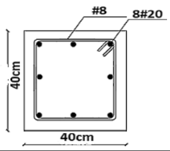	8ϕ20; ϕ8@10cm; ϕ8@20cm	35×40	5	

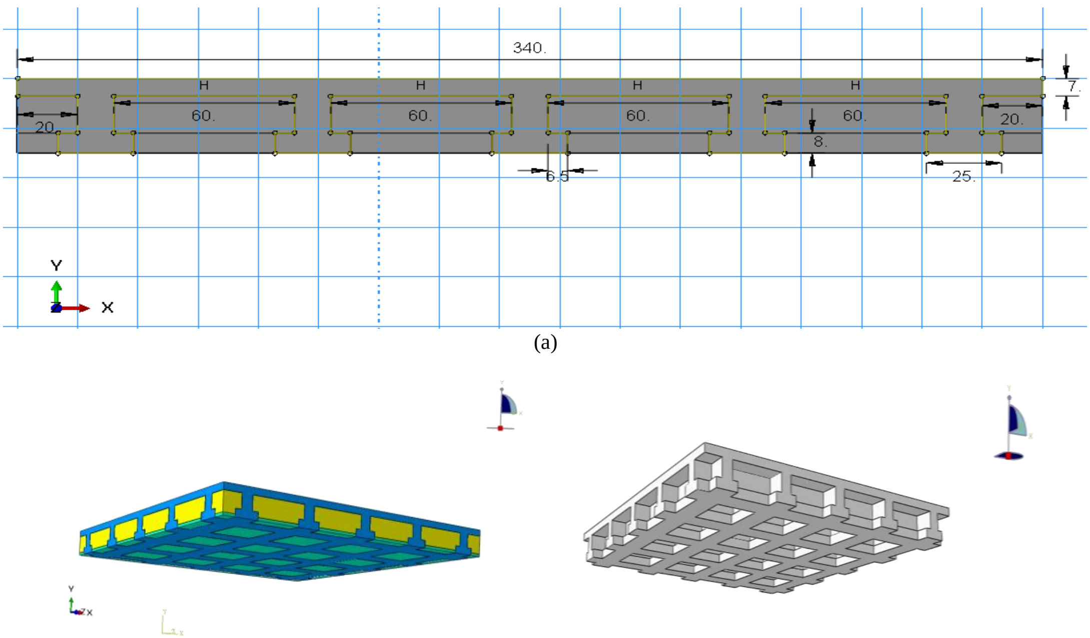

(a)

(b)

(c)

Fig.4. Geometric and completed details of the Intel-Deck roof system. (a) Geometric specifications of the joists and AAC blocks. (b) Image of the joists and their overlaying slab, excluding the AAC blocks. (C) Final and complete image of the Intel-Deck

3. Results and Discussion

3-1. Outputs of Designbuilder model for the 1st scenario

In the models developed using DesignBuilder, two separate scenarios were defined for comparison. The first scenario considered construction waste management for a residential building constructed with conventional Reinforced Concrete (RC) materials and brick walls and partitions. The second scenario evaluated the same building incorporateing an Intel-Deck roof system and walls made of autoclaved aerated concrete (AAC) blocks. The outputs obtained from the DesignBuilder simulations for both scenarios included fuel and energy consumption, as well as air and water pollutant emissions. The results related to fuel consumption for the first scenario are presented in Table 3. It should be noted that negative values indicate energy savings, energy production or recovery, energy storage, and reductions in pollutant emissions.

As can be seen in Table 3, the impact of energy recovery (electricity generation) from construction waste is reported as negative numbers. The total energy at each stage is given in the last column, which includes the sum of electrical energy consumed/generated, electrical energy saved from recycling, gasoline, diesel, and natural gas, and these values are per unit of operation. Given the low fuel consumption, the 1st scenario is environmentally acceptable in this section.

The outputs from the DesignBuilder software for the first scenario in the section related to pollutant emissions to air and water are shown in Table 4. The amount of pollutants produced depends on many factors such as the design approach, construction location, the presence of a methane gas collection system, and the composition of building materials. If energy extraction and electricity generation from the site is possible in this scenario, the amount of pollutants and greenhouse gases produced will be significantly reduced. As can be seen in Table 4, the collection, control, and extraction of gas from the construction site in this scenario reduces the emission of pollutants into the atmosphere, which is indicated by a negative sign. Also, the highest emissions of pollutants released into the air are related to carbon dioxide and methane, which also play a major role in global warming.

According to Table 4, the use of a waste collection and transportation system at the landfill stage has reduced the release of pollutants into water, which is indicated by a negative sign. At the same time, the high oxygen consumption indices at the landfill (BOD and COD) indicate that the surface and groundwater of the area are polluted by construction materials, although attempts have been made to reduce their release by using a construction waste collection system. The most produced pollutants in this sector are ammonium, chlorinated hydrocarbons, and fluoride, respectively.

3-2. DesignBuilder Model Outputs for the 2nd Scenario

In the second scenario, which concerns the use of AAC components in Intel-Deck roofs as well as the walls and partitions, the amount of energy consumed/produced and the pollutant release into water and air have been calculated separately in each sector. The results of the DesignBuilder software for the second scenario in the fuel consumption (energy) section are shown in Table 5. Table 5 shows the amounts of electricity, diesel, and natural gas consumed, as well as the electricity generated in the sorting, biological processing, waste, and recycling stages.

For the case of using AAC materials, by providing the possibility of energy recovery and electricity generation, as well as recycling, it has improved the environmental performance of the 2nd scenario in this section by saving the amount of energy consumed, which is indicated by a negative sign in Table 5. In general, recycling can reduce the amount of raw material consumption and reduce energy consumption in the material production plant as well as the energy used to transport raw materials, etc. Also, the use of AAC technology, which does not require high energy and allows for material recovery, makes this part of the scenario environmentally acceptable.

The outputs from the DesignBuilder software for the second scenario in the section on pollutant emissions to air and water are shown in Table 6. According to Table 6, the amount of pollutant emissions to air has been estimated for the stages of sorting, biological processing, waste disposal, and recycling. In this section, AAC materials have reduced the emission of pollutants into the air by providing the possibility of using a waste collection system. Recycling can reduce the consumption of raw materials and therefore reduce the production of pollutants. The negative sign indicates the reduction of pollutant emissions or energy savings, which shows the reducing effect of the relevant disposal method on pollutant emissions; this reduction is compared to the case where this method is not implemented. In Table 6, the most pollutants emitted into the air during the separation, biological processing and waste disposal stages are carbon dioxide and methane, respectively. Given the high rate of recyclability, the global warming potential of AAC materials is much lower than that of conventional brick materials.

Table 3. Outputs of the DesignBuilder model for the first scenario in the fuel consumption section

	Units	Collection	Sorting	Biological	Thermal	Landfill	Recycling	Total
Elec-Consumed	kWh	0	0	0	0	153,815	NA	153,815
Elec-Generated	kWh	NA*	NA	0	0	4,030,571	NA	4,030,571
Elec-Recycling	kWh	NA	NA	NA	NA	NA	0	0
Petrol	litres	0	NA	NA	NA	NA	NA	0
Diesel	litres	0	0	0	0	52,517	0	52,517
Nat-gas	m^3	NA	0	NA	0	NA	NA	0
Total	GJ	0	0	0	0	-36,311	0	-36,311

Table 4. Outputs of the DesignBuilder model for the first scenario in the section of pollutant emissions into air (top) and water (bottom)

	Units	Collection	Sorting	Biological	Thermal	Landfill	Recycling	Total
BOD	g	0	0	0	NA	15,305,148	0	15,305,148
COD	g	0	0	0	NA	15,297,790	NA	15,297,790
SuspendedSolids	g	0	0	0	NA	-397,176	0	-397,176
TOC	g	0	0	0	NA	-109,270	0	-109,270
AOX	g	0	0	0	NA	12,339	0	12,339
Chlorinated HC	g	0	0	0	NA	6,359	0	6,359
Dioxins/Furans	g	0	0	0	NA	0	0	0
Phenols	g	0	0	0	NA	1,462	0	1,462
Aluminium	g	0	0	0	NA	-702,972	0	-702,972
Ammonium	g	0	0	0	NA	116,832	0	116,832
Arsenic	g	0	0	0	NA	-1,318	0	-1,318
Barium	g	0	0	0	NA	-70,365	0	-70,365
Cadmium	g	0	0	0	NA	41	0	41
Chlorid	g	0	0	0	NA	-6,089,556	0	-6,089,556
Chromium	g	0	0	0	NA	-6,622	0	-6,622
Copper	g	0	0	0	NA	-3,123	0	-3,123
Cyanide	g	0	0	0	NA	-46	0	-46
Fluoride	g	0	0	0	NA	2,410	0	2,410
Iron	g	0	0	0	NA	-352,840	0	-352,840
Lead	g	0	0	0	NA	-3,859	0	-3,859
Mercury	g	0	0	0	NA	2	0	2
Nickel	g	0	0	0	NA	-2,465	0	-2,465
Nitrate	g	0	0	0	NA	-20,608	0	-20,608
Phosphate	g	0	0	0	NA	-41,370	0	-41,370
Solphate	g	0	0	0	NA	-7,887,087	0	-7,887,087
Solphide	g	0	0	0	NA	-208	0	-208
Zinc	g	0	0	0	NA	-2,855	0	-2,855
Particulates	g	0	0	0	0	-1,892,063	0	-1,892,063
CO	g	0	0	0	0	4,998,484	0	4,998,484
CO2	g	0	0	0	0	13,790,132,185	0	13,790,132,185
CH4	g	0	0	0	NA	2,105,836,223	0	2,105,836,223
Nox	g	0	0	0	0	-180,400	0	-180,400
GWP	g	0	0	0	0	58,007,719,234	0	58,007,719,234
N2O	g	0	0	0	NA	-16,044	0	-16,044
Sox	g	0	0	0	0	-8,380,401	0	-8,380,401
HCl	g	0	0	0	0	118,676	0	118,676
HF	g	0	0	0	NA	40,920	0	40,920
H2S	g	0	0	0	0	1,075,732	0	1,075,732
TotalHC	g	0	0	0	0	11,061,785	0	11,061,785
Chlorinated HC	g	0	0	0	NA	241,640	0	241,640
Dioxins/Furans	g	0	0	0	NA	0	0	0
Ammonia	g	0	0	0	NA	-4,689	0	-4,689
Arsenic	g	0	0	0	NA	0	0	0
Cadmium	g	0	0	0	0	-5	0	-5
Chromium	g	0	0	0	NA	4	0	4
Copper	g	0	0	0	0	0	0	0
Lead	g	0	0	0	0	-328	0	-328
Manganese	g	0	0	0	0	-153	0	-153
Mercury	g	0	0	0	0	-47	0	-47
Nickel	g	0	0	0	0	-2,216	0	-2,216
Zinc	g	0	0	0	NA	-108	0	-108

Table 5. Outputs of the DesignBuilder model for the second scenario in the fuel section

	Units	Collection	Sorting	Biological	Thermal	Landfill	Recycling	Total
Elec-Consumed	kWh	0	263,588	1,331,715	0	19,446	NA	1,614,479
Elec-Generated	kWh	NA	NA	0	0	1,334,153	NA	-1,334,153
Elec-Recycling	kWh	NA	NA	NA	NA	NA	27,214,087	27,214,087
Petrol	litres	0	NA	NA	NA	NA	NA	0
Diesel	litres	0	116	930	0	9,364	4,599	15,009
Nat-gas	m^3	NA	2,109	NA	0	NA	NA	2,109
Total	GJ	0	2,760	13,426	0	-12,738	-273,421	-269,742

The absence of the need to transport waste to material manufacturing plants in this scenario reduces greenhouse gas emissions.

According to Table 6, using the waste collection and transportation system, there is a reduction in the release of pollutants into the aquatic environment. Also, recycling waste by reducing the consumption of raw materials has reduced the release of pollutants into water. The effect of recycling, which reduces AOX (absorbable halogenated organic compounds) and COD, is indicated by a negative sign. Due to the need for moisture in AAC parts, the amount of water pollution is high in terms of BOD and COD indices in the biological processing stage. However, due to the prevention of material transfer to construction sites, the 2nd scenario causes less pollution than if all construction materials are sent to the landfill. Also, in this stage, the release of heavy metals such as zinc, nickel, lead, iron, copper, chromium, cadmium is higher than in other stages.

Table 6. Outputs of the DesignBuilder model for the second scenario in the section of pollutant emissions in air (top) and in water (bottom)

	Units	Collection	Sorting	Biological	Thermal	Landfill	Recycling	Total
BOD	g	0	26	2,599,237	NA	2,813,936	3,780,532	9,193,732
COD	g	0	527	4,396,677	NA	2,811,440	-114,179,089	-106,968,445
SuspendedSolids	g	0	37,245	188,274	NA	-155,336	7,094,573	7,164,765
TOC	g	0	8,444	41,789	NA	-36,985	7,328,381	7,341,629
AOX	g	0	1	7	NA	5,108	-1,183,806	-1,178,690
Chlorinated HC	g	0	0	2	NA	2,158	357	2,517
Dioxins/Furans	g	0	0	0	NA	0	0	0
Phenols	g	0	60	304	NA	557	-1,998	-1,076
Aluminium	g	0	47,861	241,482	NA	-238,397	-1,260,238	-1,209,292
Ammonium	g	0	926	453,905	NA	34,721	27,783	517,335
Arsenic	g	0	96	483	NA	-439	-2,689	-2,549
Barium	g	0	4,790	24,173	NA	-23,863	-106,828	-101,729
Cadmium	g	0	3	16	NA	11	-18	12
Chlorid	g	0	529,710	2,682,389	NA	-2,119,360	38,618,350	39,711,090
Chromium	g	0	476	2,402	NA	-2,174	-13,765	-13,061
Copper	g	0	235	1,187	NA	-997	-3,804	-3,378
Cyanide	g	0	3	16	NA	-16	-3,371,816	-3,371,813
Fluoride	g	0	0	0	NA	947	-226	721
Iron	g	0	64,024	323,373	NA	-147,938	-129,428	110,032
Lead	g	0	289	1,459	NA	-1,307	-6,641	-6,199
Mercury	g	0	0	0	NA	1	6	7
Nickel	g	0	239	1,208	NA	-673	-6,596	-5,822
Nitrate	g	0	1,401	7,080	NA	-6,989	2,085,012	2,086,504
Phosphate	g	0	2,817	14,211	NA	-14,030	-24,949	-21,951
Solphate	g	0	539,780	2,725,728	NA	-2,682,021	14,792,181	15,375,668
Solphide	g	0	14	71	NA	-70	79	94
Zinc	g	0	481	2,424	NA	-641	-12,824	-10,560
Particulates	g	0	134,845	681,463	0	-652,334	-2,839,041	-2,675,068
CO	g	0	17,814	95,605	0	4,998,484	-15,534,082	-13,900,722
CO2	g	0	113,945,992	574,956,748	0	4,526,972,607	5,163,585,396	52,289,951
CH4	g	0	269,283	1,355,340	NA	696,988,366	-6,564,025	692,048,964
Nox	g	0	249,896	1,275,817	0	-523,831	-22,142,137	-21,140,153
GWP	g	0	119,940,424	605,127,823	0	19,162,041,422	5,274,323,759	14,612,785,911
N2O	g	0	1,095	5,513	NA	-5,442	14,332	88,606
Sox	g	0	595,870	3,011,097	0	-2,881,479	906	-10,179,447
HCl	g	0	20,067	101,384	0	36,838	781	172,621
HF	g	0	1,972	9,962	NA	13,309	0	26,149
H2S	g	0	0	0	NA	356,076	0	365,858
TotalHC	g	0	0	0	NA	3,661,545	0	3,661,545
Chlorinated HC	g	0	0	0	NA	79,985	79,985	79,985
Dioxins/Furans	g	0	0	0	0	0	235,004	0
Ammonia	g	0	319	1,611	NA	-1,590	-1,590	235,344
Arsenic	g	0	0	0	0	0	0	0
Cadmium	g	0	2	12	0	-2	-93	-80
Chromium	g	0	0	0	0	1	36	38
Copper	g	0	0	0	0	0	196	196
Lead	g	0	24	122	0	-111	3,501	3,536
Manganese	g	0	10	53	NA	-52	0	11
Mercury	g	0	3	16	0	-16	3	7
Nickel	g	0	151	761	0	-751	-1,470	-1,310
Zinc	g	0	35	176	0	-40	-90	81

In general, the highest release of pollutants into water is related to the landfill stage. For easier comparison and better understanding, the final data for each scenario in the fuel consumption and air and climate emission sections are given in Tables 7 to 9.

The highest diesel fuel consumption is related to the 1st scenario. However, the first scenario has the lowest electrical energy consumption. Also, the highest carbon dioxide and methane production belongs to the first scenario. In the section of pollutant emissions in water, the amount of biological oxygen demand (BOD) is high and significant in both scenarios. Also, the emission of fluoride and ammonium in water in all scenarios and the emission of nitrate and sulfate in the second scenario have played the most significant role in the pollution of this section.

Here, it is necessary to clarify that the compressive strength of clay brick typically ranges from 3 to 10 MPa, with a density of approximately 1500–1900 kg/m³ [29,30]. In contrast, AAC materials exhibit a compressive strength of about 3–7 MPa and a density in the range of 300–800 kg/m³ [29,31]. Accordingly, the strength-to-density ratio of brick and AAC materials falls within 0.1–0.6% and 0.6–20%, respectively.

Table 7. Energy consumed in different scenarios per unit of operation (tonnage of building materials produced per year)

Parameter	Units	1st Senario	2nd Senario
Comsumed electricity	kWh	153815	1614749
Generated electricity	kWh	-4030571	-1334153
Recycled electricity- Recycling stage	kWh	0	-27214087
Diesel fuel	L	52517	15009
Natural Gas	m^3	0	2109
Total	GJ	-36311	-269742

Table 8. Emission of pollutants into the air per unit of operation (tonnage of building materials produced per year)

Pollutants	Units	1st Senario	2nd Senario
Suspended Solids (PM10)	g	1892063	-2675068
Carbon Monoxide (CO)	g	4998484	-13900722
Carbon Dioxide (CO_2)	g	137901321185	52289951
Methane (CH_4)	g	2105836223	692048964
Nitrogen Oxides (NO_X)	g	-180400	-21140153
Nitrous Oxide (N_2O)	g	-16044	88606
Oxides Sulfur (SO_X)	g	-8380401	-10179447
Hydrochloric Acid (HCl)	g	118676	172621
Hydrogen sulfide (H_2S)	g	1075732	356858
Hydrofluoric Acid (HF)	g	40920	26149
Ammonia (NH_3)	g	04689	235344
Arsenic (As)	g	0	0
Cadmium (Cd)	g	-5	-80
Chromium (Cr)	g	4	38
Copper (Cu)	g	0	196
Lead (Pb)	g	-328	3536
Manganese (Mn)	g	-153	11
Mercury (Hg)	g	-47	7
Nickel (Ni)	g	-2216	-1310
Zink (Zn)	g	-108	81
Total Hydrocarbons	g	11061785	3661545
Chlorinated Hydrocarbons	g	241640	79985

Table 9. Emission of pollutants into the water per unit of operation (tonnage of building materials produced per year)

Pollutants	Units	1st Senario	2nd Senario
Biological Oxygen Demand (BOD)	g	15305148	9193732
Chemical Oxygen Demand (COD)	g	15297790	-106966445
Ammonium (NH_4)	g	116832	517335
Arsenic (As)	g	-1318	-2549
Barium (Ba)	g	-70365	-101729
Cadmium (Cd)	g	41	12
Chromium (Cr)	g	-6622	-13061
Copper (Cu)	g	-3123	-3378
Lead (Pb)	g	-3859	-6199
Mercury (Hg)	g	2	7
Nickel (Ni)	g	-2465	-5822
Nitrate ($-NO_3$)	g	-20608	2086504
Phosphate ($PO^3{}_4$)	g	-41370	-21951
Sulphate ($SO^2{}_4$)	g	-7887087	15375668
Sulphide ($SO^{-2}{}_3$)	g	-208	94
Zink (Zn)	g	-2855	-10560
Suspended solids (ss)	g	-397176	7164756
Total Organic Carbon (TOC)	g	-109270	7341629
AOX	g	12339	-1178690
Chlorinated Hydrocarbon	g	6359	2517
Phenol	g	1462	-1076
Chloride	g	-6089556	39711090
Cyanide	g	-46	-3371813
Fluoride	g	2410	721
Iron	g	-352840	110032
Aluminum	g	-702972	-1209292

Therefore, in addition to their environmental advantages, AAC materials demonstrate a higher relative strength compared with traditional clay bricks.

3-3. Life Cycle Inventory (LCI)

In this section, the information and results collected in the DesignBuilder software were introduced to the software using the openLCA database. The results of the environmental impact assessment of both scenarios in different impact classes are given in Table 10. The results of the life cycle inventory are consistent with the results obtained in the previous section and it can be seen that the first scenario was reported to be more destructive in terms of the effects on global warming, ozone layer depletion and fossil fuel consumption than the second scenario (i.e. AAC).

Table 10. Results of the environmental impact assessment of two scenarios using the TRACI method

Impact Class	Units	1st Senario	2nd Senario
Acidification	Kg SO_2 eq	2.83E+02	-2.53405E-06
Ecotoxicity	CTUe	-4.70721E-09	-3.16626E-09
Eutrophication	Kg N eq	1.12E+02	-1.76626E-06
Global warming	Kg CO_2 eq	4.33E+06	1.13E+06
Human health carcinogenic	CTUh	-3.395412797	-34.26333823
Human health non-carcinogenic	CTUh	-0.076397112	-0.164690382
Ozone layer depletion	Kg CFC-11 eq	6.13E-05	1.75E-05
Photochemical smog	Kg O_3 eq	2.53E+03	-9.60922E-09
Fossil fuel depletion	MJ Surplus	3.09E+05	9.93E+04
Respiratory effects	Kg PM2.5 eq	-2.87894E-05	-6.08587E-06

According to the results reported in the studies of Fouad et al. [14] and Shi et al. [15], who evaluated the environmental impacts of AAC materials in different countries using the LCA method, the energy consumed and carbon dioxide released in the use of conventional concrete is higher than AAC. This is also consistent with the results obtained in this study.

3-4. Results of FEM analysis in ETABS

3-4-1. Drifts

Figure 5 shows the maximum floor displacement values for the 3- and 5-story structures together with the allowable drift limit according to the Iranian Code of Practice for Seismic Resistant Design of Buildings (Standard No. 2800, 4th Edition). The maximum lateral deflection in the 3-story model with the SLAB section was 0.003617 cm at the second floor, representing a reduction of more than 35% compared to the DECK roof model (0.005016 cm). This reduction is attributed to the flexural stiffness of the SLAB element, which models the combined membrane–bending behavior of the Intel-Deck roof system. In actual Intel-Deck roofs, the structural configuration consists of orthogonal reinforced concrete ribs forming an asymmetrical I-shaped cross-section integrally within the slab, as previously described. These ribs (commonly referred to as the I-shaped members of the system) are not separate steel beams but part of the monolithic reinforced concrete roof system, and they contribute to the lateral stiffness of the structure. Similarly, in the 5-story frame, the maximum lateral deflection in the SLAB model was 0.004157 cm at the third floor, showing a reduction of more than 21% compared to the DECK section (0.005057 cm). According to Figure 4, while the DECK model reached the allowable drift limit, the SLAB model remained below the code limit, with at least a 24% reduction.

Figure 6 shows the torsional force diagram of the third roof of a three-story structure under lateral load in the x direction. As can be seen in Figure 5, for the DECK model, the torsional forces of the beams were very small (on average t.m 0.005), while for the SLAB model, relatively large values of the torsional force of the beams were recorded (t.m 1.2). Since the roof of the SLAB model contributes to the lateral stiffness, the bending force created in the Intel-Deck roof bending element caused the torsional force in the floor beams.

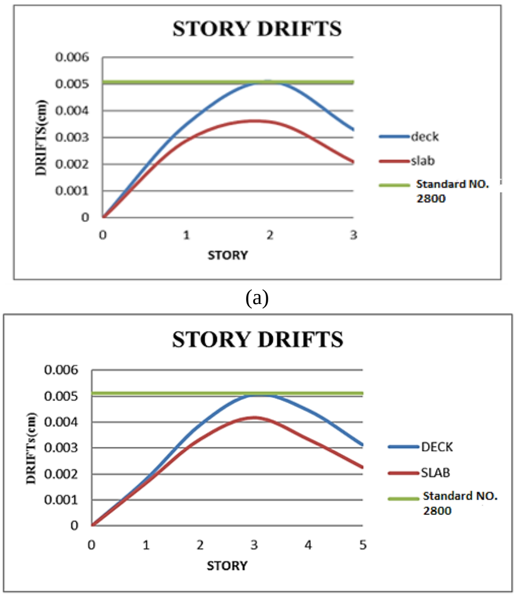

(a)

(b)

Fig.5. Lateral deflection of stories in: (a) 3-story frame; (b) 5-story frame

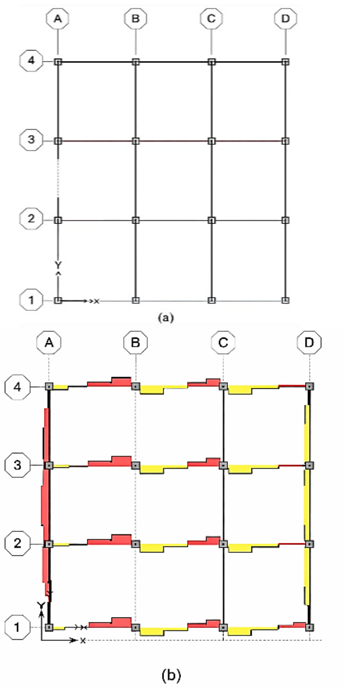

(a)

(b)

Fig. 6. Torsional force diagram of beams under X-axis earthquake load in the model with: (a) DECK; (b) SLAB roof.

In other words, the membrane-behavior roof model (DECK section) is not able to calculate the correct values of the torsional forces and torsional reinforcement in the beams.

3-4-2. Reinforcement size

Table 11 shows the calculated longitudinal reinforcement values for the second story in two models with DECK and SLAB roofs. In the model with SLAB section, in terms of the roof contribution to the lateral stiffness, the contribution of the roof beams and, consequently, the forces generated in the beams were significantly reduced compared to the model with DECK section, and this resulted in a reduction in the area of the longitudinal reinforcement of the beams (a reduction of about 14%). In other words, the use of SLAB section reduced the reinforcement consumed in the beam sections. These results are consistent with previous studies conducted by Reirz-Kojichi et al. [16].

Table 12 tabulates the shear reinforcement values calculated for the A-B span beam in the 3-story structure with DECK and SLAB roof sections. It can be seen that the use of SLAB section reduced the required shear reinforcement in the beam sections (about 10%). Figure 7 shows the shear force diagram for the two different DECK and SLAB cases for the last floor in the 5-story frame. The diagrams in Figure 6, also indicate that the roof model with SLAB section had lower shear forces than the DECK model and the shear force distribution in the SLAB section was more uniform than the DECK section.

3-5. Equivalent Thickness

Here, FEM modeling by ABAQUS software was used to determine the equivalent thickness for the roof's cross section. According to Figure 8, the frame model was created in the ABAQUS finite element package, in which in one series of models, the roof with AAC blocks was used, and in the other series, the Intel-Deck roof with different thicknesses of 5, 10, 14, 15 and 20 cm was created. The models were analyzed under quasi-statical loading conditions with a total lateral loading of 1000 kg at the top roof level. The loading was distributed on the lateral surface of the roof beams. Since in the two types of considered frames, other structural components have the same characteristics, assuming the same lateral stiffness in the two roofs, the lateral displacement of the two frames should also be equivalent.

Table 11. Values of longitudinal reinforcement (mm^2) for the beam on A-B axis

Position	deck right	Deck- middle	Deck-left	Slab-left	Slab-middle	Slab-right
A-B row 4 top	4,502	1,443	4,477	3,386	0.914	3,568
A-B row 4 bot	3,568	2,576	3,139	1,979	1,669	1,843
A-B row 3 top	5,314	1,758	5,536	3,281	0.946	3,568
A-B row 3 bot	3,568	3,568	3,568	1,908	2,334	3,568
A-B row 2 top	5,314	1,758	5,536	3,281	0.946	3,568
A-B row 2 bot	3,568	3,568	3,568	1,908	2,334	3,568
A-B row 1 top	4,502	1,443	4,477	3,281	0.914	3,568
A-B row 1 bot	3,568	2,576	3,139	1,908	2,334	3,568

Table 12. Shear reinforcement for the beam on A-B axis

Position	DECK- right	DECK- middle	DECK- left	SLAB- left	SLAB- middle	SLAB- right
row 4	0.092	0.073	0.095	0.087	0.072	0.091
row 3	0.0118	0.085	0.012	0.097	0.074	0.103

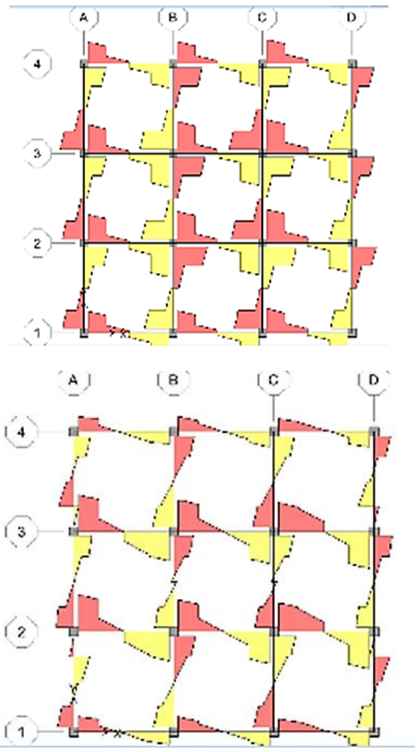

Fig. 7. Shear force diagram for the section: (a) DECK; (b) SLAB

In this approach, firstly, the lateral displacement value of the frame model with a roof containing AAC components was determined in ABAQUS. Then, in the next step, by selecting different values for the Intel-Deck roof thickness (t), through a trial-&-error process, the same lateral displacement was found in both frames.

Tables 13 to 15 show the displacement and lateral stiffness results for 1, 2 and 3 story models. It is important to note that the models with Intel-Deck roofs are named with the letter S, the first digit from the left is the number of stories, the next two digits are the number of spans in the x and y directions, and the two digits on the right represent the equivalent thickness of the slab. For example, S12205 is a 1-story frame model with Intel-Deck roof system and two spans in each direction with a thickness of 5 cm for the slab. Also, the models with AAC roofs are named with the word Deck, the first digit from the left is the number of stories and the next digit is the number of spans. For example, Deck32 is a 3-story frame model with two openings in each direction.

After a trial-and-error procedure, the equivalent thickness of the roof with a SLAB section was estimated to be about 15 cm. For the present examples, under a lateral load of 1 ton, the lateral displacement of a 1-story, 1-span frame with the AAC roof is calculated to be 0.57 cm and that is 0.5812 cm for the model with Inteldeck roof of 15 cm thickness (less than 3% difference).

The maximum lateral displacement and calculated stiffness for the frame models are plotted in in Figure 8. According to Figure 9-(a) and Table 13, the displacement of the 1-story, 2-span frame with AAC-paneled roof was 0.1184 cm, which is close to the displacement of the 15 cm Inteldeck roof (S15) (displacement 0.1181 cm and a difference of about 2%) and can be substituted as an equivalent section. It is worth noting that the 2-span frames with 14 and 16 cm Inteldeck roofs (S14 and S16) also have a response close to the AAC roof, but due to implementation issues, choosing a roof thickness of 15 cm is more practical. On the other hand, the stiffness of the 1-story, 2-span model with AAC roof was 84.45 tons/cm, and the stiffness of the model with 15 cm thick Inteldeck roof (S15) was 84.67 tons/cm, which were close to each other and could be replaced as equivalent sections.

According to the trend of the graphs in Figure 9, it is clear that increasing the thickness of Inteldeck roofs increases the lateral stiffness of the frame. According to Figure 8 and Tables 14 and 15, the displacement and stiffness of the 2-span model with AAC roof and 15 cm thick Inteldeck roof (S15) in the 2- and 3-story frames were also close to each other and could be replaced as equivalent sections. In the two-story models, the roof displacement in the AAC and Inteldeck models with a thickness of 15 cm (S22215) was 0.02401 and 0.02407 cm, respectively, which is a difference of about 3%. Also, in the 3-story, 2-span model, the roof displacement was 0.6498 and 0.6489 cm, respectively, in the AAC and Inteldeck roof models with a thickness of S32215, which is a difference of about 2% and can be equated with each other.

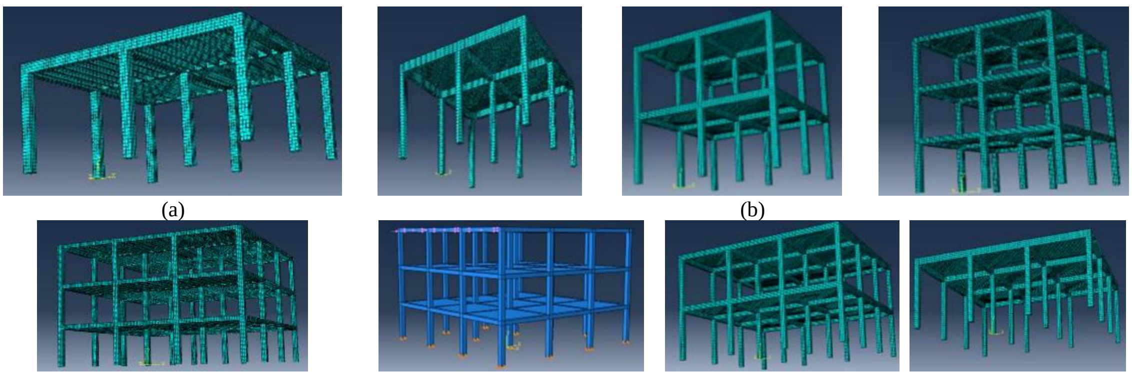

Fig. 8. Frame models in ABAQUS: (a) 2-span 1-story with roof with AAC components; (b) 2-span with equivalent Inteldeck roof; (c) 3-span 3-story with roof with AAC components; (d) 3-span with equivalent Inteldeck roof

Table 13. Displacement and lateral stiffness of 1-story frames

Frame model	**S12205**	**S12210**	**S12214**	**S12215**	**S12216**	**S12220**		
u1 (cm) Displacement	0.01298	0.01228	0.01189	0.01181	0.01176	0.01138		
k1 (t/cm) Stiffness	77.04	81.43	84.1	84.67	85.03	87.87		
Frame model	**Deck12**	**S13305**	**S13310**	**S13314**	**S13315**	**S13316**	**S13320**	**deck13**
u1 (cm) Displacement	0.01184	0.01456	0.01416	0.01358	0.01335	0.01321	0.01271	0.01351
k1 (t/cm) Stiffness	84.45	68.68	70.62	73.37	74.9	75.7	78.67	74.01

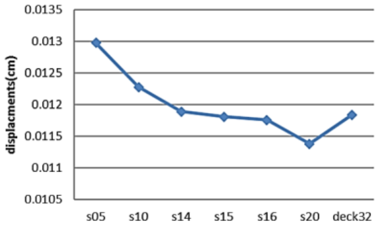

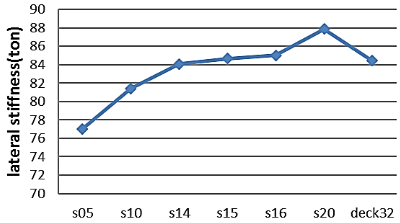

Table 14. Displacement and lateral stiffness of 2-story frames

Frame model	**S22205**	**S22210**	**S22214**	**S22215**	**S22216**	**S22220**		
u1 (cm) Displacement	0.02654	0.02512	0.02433	0.02407	0.0241	0.02339		
k1 (t/cm) Stiffness	37.67	39.8	41.01	41.54	41.49	42.75		
Frame model	**Deck22**	**S23305**	**S23310**	**S23314**	**S23315**	**S23316**	**S23320**	**Deck23**
u1 (cm) Displacement	0.02401	0.04315	0.03854	0.03154	0.03012	0.02931	0.02658	0.02994
k1 (t/cm) Stiffness	41.69	23.17	25.94	31.7	33.2	34.11	37.62	33.4

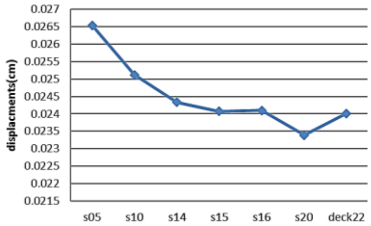

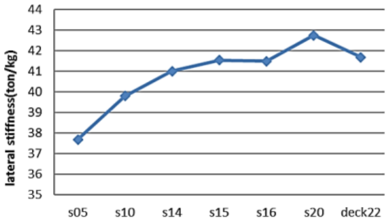

Table 15. Displacement and lateral stiffness of 3-story frames

Frame model	**S32205**	**S32210**	**S32214**	**S32215**	**S32216**	**S32220**		
u1 (cm) Displacement	0.07251	0.06688	0.06502	0.06489	0.06435	0.06148		
k1 (t/cm) Stiffness	13.79	14.51	15.37	15.41	15.54	16.26		
Frame model	**Deck32**	**S33305**	**S33310**	**S33314**	**S33315**	**S33316**	**S33320**	**Deck33**
u1 (cm) Displacement	0.06498	0.06951	0.06568	0.06181	0.06122	0.06103	0.05959	0.06158
k1 (t/cm) Stiffness	15.38	14.38	15.22	16.17	16.33	16.38	16.78	16.23

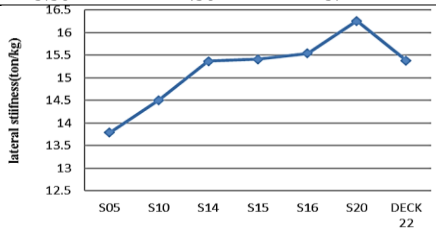

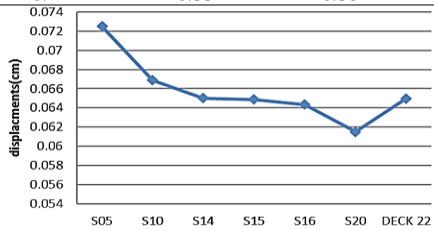

In the 3-span models, the displacement and stiffness of the frame with the AAC roof (Deck13) and the Inteldeck roof with a thickness of 15 cm (S13315) were 0.01351 and 0.01335 cm, and 74.01 and 74.9 tons/cm, respectively (a difference of about 2-3%), which can be equated with each other. In all three-span models, the difference in lateral displacement and stiffness in the model with an AAC roof with a roof equivalent to 15 cm thick was less than 5%.

4. Conclusions

The main idea of this research was to evaluate the feasibility of using autoclaved aerated concrete (AAC) blocks as a replacement for the conventional blocks used in the Inteldeck roof system. In this study, the life cycle assessment approach was used as a tool to evaluate the benefits of using AAC materials in construction. For this purpose, two construction waste management scenarios were considered, which included the use of AAC materials and clay bricks. And the DesignBuild software was used to calculate the environmental load of each scenario. In the next step, modeling of different building frames with the Inteldeck roof system with AAC block components was performed in the ETABS software using two DECK and SLAB sections for the roof. Also, by modeling building frames with different numbers of floors and spans in the ABAQUS finite element software, the equivalent thickness of the roof with AAC components with the Inteldeck roof was determined. The most important results obtained are as follows:

1- The AAC application scenario had a lower environmental burden than brick materials at different global warming and resource consumption fields.

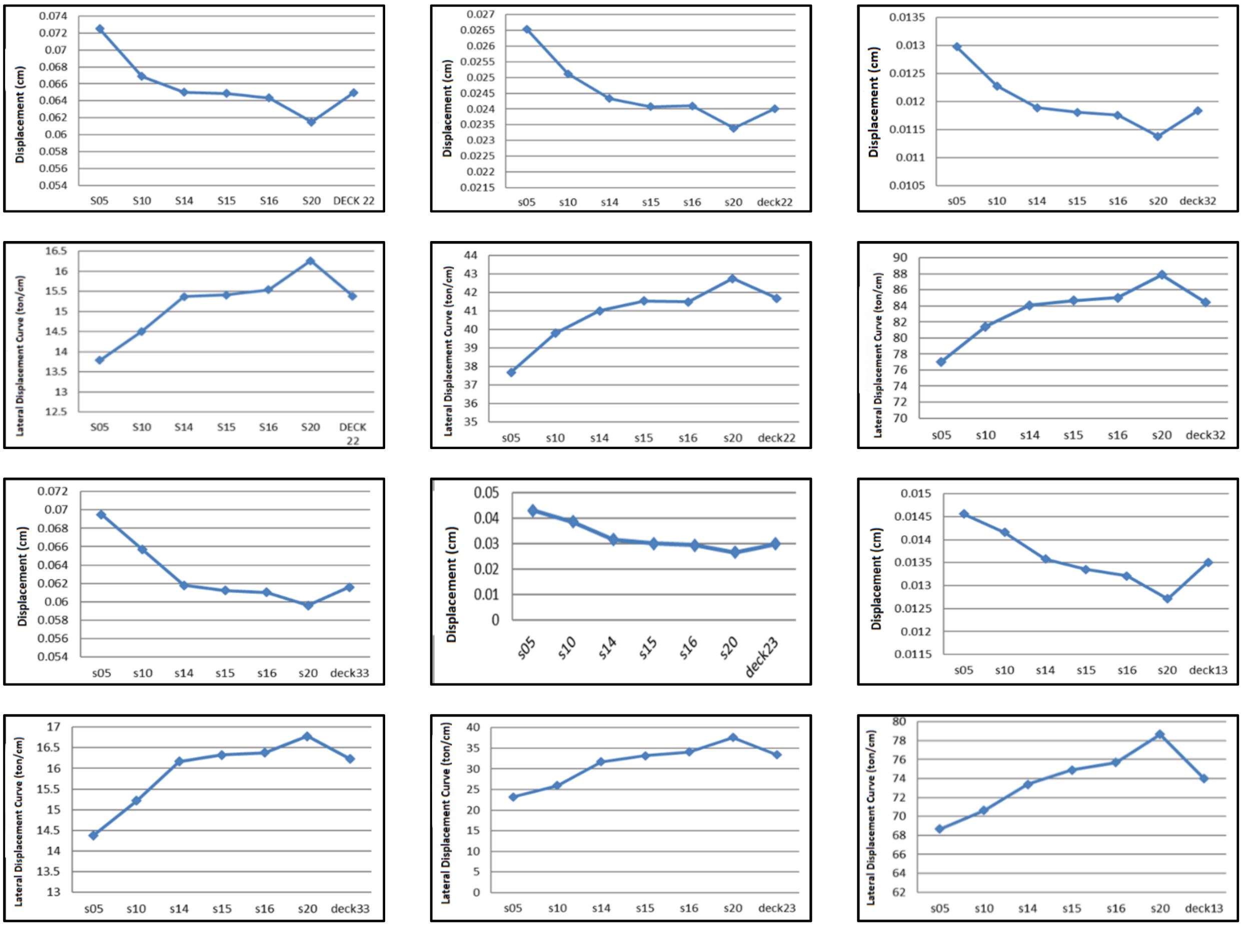

Fig.9. Displacement and lateral stiffness of frames with: (a) 2-span 1-story; (b) 2-span, 1-story; (c) 2-span, 3-story; (d) 3-span, 1-story; (e) 3-span, 2-story; (f)) 3-span, 3-story

2- According to the outputs of the DesignBuilder model, as the rate of separation and recycling of construction waste increased, the amount of environmental pollutants also decreased due to the increase in the amount of recycled materials and the prevention of the emission of pollutants resulting from the production of raw materials. As a result, in terms of sustainability indicators, separation and recycling of materials was the first priority, and traditional approaches such as landfilling waste were the next priority.

3- The Inteldeck roof made with AAC components had a combined flexural-membrane behavior that could contribute to the lateral stiffness of the structure. This type of roof in a real building, with a set of asymmetrical I-beams, has a bending behavior and contributes to the lateral stiffness. As a result, this roof system as a structural element changes the distribution of internal forces. This should be considered in the modeling of the building software. The FILLED DECK element in the ETABS software library was unable to model the behavior of these roofs.

4- Modeling the roof with AAC components using the SLAB section caused the roof system to participate in the lateral load of the frame and, as a result, reduced the lateral displacement. In the 3D models of the building frame, a reduction in the lateral displacement of the floors was observed in the modeling mode with the SLAB element compared to the FILLED DECK element. As a result, it can be stated that the bending force created in the bending element of the Intel Deck roof causes a torsional force in the floor beams. While, the roof model with membrane behavior (DECK section) was unable to calculate the correct values of the torsional forces and torsional reinforcements in the beams. Also, modeling the roof with AAC elements with SLAB elements reduced the area of longitudinal reinforcement of the beams by about 14%.

5- By modeling the reinforced concrete frames in the ABAQUS finite element software with the conventional Intel Deck roof system and the roof with AAC elements, the equivalent thickness of the Slab section to replace the Deck section in the ETABS program models was obtained as 15 centimeters.

5. References

[1] Pawar, A. J., Patil, Y. D., Vesmawala, G. R., Dhake, P. D., & Nikam, J. S. (2024, June). Investigating the flexural behaviour of biaxial voided slab with varying size and spacing of cuboidal shaped void formers with innovative type of fixing reinforcement. In *Structures* (Vol. 64, p. 106616). Elsevier.

[2] Intel-Deck, (2020). Available at: https://intelldeck.com/ & https://inteldeck.ir/ [Accessed 01.10.2023].

[3] Thienel, K. C., Haller, T., & Beuntner, N. (2020). Lightweight concrete—From basics to innovations. *Materials*, 13(5), 1120.

[4] Hanečka, K., Koronthályová, O. G., & Mšovský, P. M. (1997). The carbonation of autoclaved aerated concrete. *Cement and concrete research*, 27(4), 589-599.

[5] Houben, H., & Guillaud, H. (1994). *Earth construction: a comprehensive guide*. London, UK: Intermediate Technology Publications.

[6] Raj, A., Borsaikia, A. C., & Dixit, U. S. (2020). Evaluation of mechanical properties of autoclaved aerated concrete (AAC) block and its masonry. *Journal of The Institution of Engineers (India): Series A*, *101*(2), 315-325.

[7] Chen, J., Huang, Y., Liu, G., Chen, H., Liang, Y., Rashad, A. M., ... & Wang, W. (2025). Performance regulation of ultra-lightweight autoclaved aerated concrete by metakaolin and its impact on energy efficiency in thermal insulation walls. *Energy and Buildings*, 116374.

[8] Kadashevich, I., Schneider, H. J., & Stoyan, D. (2005). Statistical modeling of the geometrical structure of the system of artificial air pores in autoclaved aerated concrete. *Cement and Concrete Research*, 35(8), 1495-1502.

[9] Kus, H. (2003). Long-Term Performance of Water Repellents on Rendered Autoclaved Aerated Concrete. *Restoration of Buildings and Monuments*, 9(1), 23-40.

[10] Shi, Y., Li, Y., Tang, Y., Yuan, X., Wang, Q., Hong, J., & Zuo, J. (2019). Life cycle assessment of autoclaved aerated fly ash and concrete block production: a case study in China. *Environmental Science and Pollution Research*, *26*(25), 25432-25444.

[11] Wang, C. L., Ni, W., Zhang, S. Q., Wang, S., Gai, G. S., & Wang, W. K. (2016). Preparation and properties of autoclaved aerated concrete using coal gangue and iron ore tailings. *Construction and Building Materials*, 104, 109-115.

[12] Kunchariyakun, K., Asavapisit, S., & Sombatsompop, K. (2015). Properties of autoclaved aerated concrete incorporating rice husk ash as partial replacement for fine aggregate. *Cement and concrete composites*, 55, 11-16.

[13] Galman, I., & Jasiński, R. (2023). Morphology of cracks and comparison of load-bearing capacity of joints of AAC masonry walls. *ce/papers*, *6*(2), 125-133.

[14] Fouad, F., Ramadan, W., Schoch, T., & Kirby, J. (2023). Environmental performance of autoclaved aerated concrete in the USA. *ce/papers*, *6*(2), 5-14.

[15] Shi, Y., Li, Y., Tang, Y., Yuan, X., Wang, Q., Hong, J., & Zuo, J. (2019). Life cycle assessment of autoclaved aerated fly ash and concrete block production: a case study in China. *Environmental Science and Pollution Research*, *26*, 25432-25444.

[16] Reyes-Quijije, M., Rocha-Tamayo, A., García-Troncoso, N., Baykara, H., & Cornejo, M. H. (2022). Preparation, Characterization, and Life Cycle Assessment of Aerated Concrete Blocks: A Case Study in Guayaquil City, Ecuador. *Applied Sciences*, *12*(4), 1913.

[17] Raj, A., Borsaikia, A. C., & Dixit, U. S. (2019). Manufacturing of autoclaved aerated concrete (AAC): present status and future trends. *Advances in Simulation, Product Design and Development: Proceedings of AIMTDR 2018*, 825-833.

[18] Talang, R. P. N., & Sirivithayapakorn, S. (2018). Comparing environmental burdens, economic costs and thermal resistance of different materials for exterior building walls. *Journal of Cleaner Production*, *197*, 1508-1520.

[19] Garg, R. B., & Singh, G. (2024). Exploring the Components of Green Building Envelopes for Sustainable Civil Infrastructure: A Critical Review. *Green Manufacturing and Materials Processing Methods*, 110-128.

[20] Tu, J., Chen, G., & Yu, C. (2024). Experimental study on energy saving and thermal insulation of AAC walls and sandwich structures. *Case Studies in Thermal Engineering*, *61*, 104999.

[21] Tu, J., Fang, L., Yu, C., Chen, G., Lan, J., & Zhang, R. (2025). Analysis and Research on Thermal Insulation Performance of Autoclaved Aerated Concrete Sandwich Perimeter Wall in Hot-Summer and Cold-Winter Regions Under Low Temperature Environment. *Buildings*, *15*(18), 3332.

[22] HAPPHO – Partners in Realising Happy Homes. *What Is the Cost of House Construction*? [online]. Available at: https://happho.com/ [Accessed 01 09. 2023].

[23] DesignBuilder Software Ltd. (2023). *DesignBuilder Software Packages* [online]. Available at: https://designbuilder.co.uk/ [Accessed 01 06. 2023].

[24] Cavalliere, C., Habert, G., Dell'Osso, G. R., & Hollberg, A. (2019). Continuous BIM-based assessment of embodied environmental impacts throughout the design process. *Journal of Cleaner Production*, *211*, 941-952.

[25] GreenDelta. (2023). *openLCA 2.0* [online]. Available at: https://www.openlca.org/ [Accessed 01 06. 2023].

[26] Bare, J.C., G.A. Norris, D.W. Pennington, & T. McKone. (2003). TRACI: The tool for the reduction and assessment of chemical and other environmental impact. *Journal of Industrial Ecology*. 6: 49-78.

[27] Building and Housing Research Center (BHRC). (2015). *Iranian Code of Practice for Seismic Resistant Design of Buildings: Standard No. 2800-05*, 4th Ed, Iran. (In persian)

[28] Iranian National Building Code for Structural Loading-Standard 519 (part 6), Ministry of Housing and Urban Development, Tehran, Iran, 2000. (in Persian)

[29] Masonry Standards Joint Committee. (2016). *Building Code Requirements and Specification for Masonry Structures: Containing Building Code Requirements for Masonry Structures (TMS 402-11/ACI 530-11/ASCE 5-11), and Specification for Masonry Structures TMS 402-11/ACI 530-11/ASCE 6-11), and Companion Commentaries*. ASCE: Reston, VA, USA.

[30] Murthi, P., Bhavani, M., Musthaq, M. S., Jauhar, M. O., & Devi, V. R. (2021). Development of relationship between compressive strength of brick masonry and brick strength. *Materials Today: Proceedings*, 39, 258-262.

[31] Raj, A., Borsaikia, A. C., & Dixit, U. S. (2020). Evaluation of mechanical properties of autoclaved aerated concrete (AAC) block and its masonry. *Journal of The Institution of Engineers (India): Series A*, 101, 315-325.